https://doi.org/10.2352/ISSN.2470-1173.2020.16.AVM-255

Multi-Sensor Fusion in Dynamic Environment using Evidential Grid Mapping

G. M. Dilshan P. Godaliyadda; Vijay Pothukuchi; JuneChul Roh; Texas Instruments, Dallas, TX, U.S.A.

Abstract

Grid mapping is widely used to represent the environment surrounding a car or a robot for autonomous navigation. This paper describes an algorithm for evidential occupancy grid (OG) mapping that fuses measurements from different sensors, based on the Dempster-Shafer theory, and is intended for scenes with stationary and moving (dynamic) objects. Conventional OG-mapping algorithms tend to struggle in the presence of moving objects because they do not explicitly distinguish between moving and stationary objects. In contrast, evidential OG mapping allows for dynamic and ambiguous states (e.g. a LIDAR measurement: cannot differentiate between moving and stationary objects) that are more aligned with measurements made by sensors.

In this paper, we present a framework for fusing measurements as they are received from disparate sensors (e.g. radar, camera and LIDAR) using evidential grid mapping. With this approach, we can form a live map of the environment, and also alleviate the problem of having to synchronize sensors in time. We also designed a new inverse sensor model for radar that allows us to extract more information from object level measurements, by incorporating knowledge of the sensor's characteristics. We have implemented our algorithm in the OpenVX framework to enable seamless integration into embedded platforms. Test results show compelling performance especially in the presence of moving objects.

Introduction

In recent years, environment mapping by fusing measurements from multiple disparate sensors has gained popularity especially in safety critical applications such as autonomous driving. This is because with multiple disparate sensors one can minimize or eliminate failures, by exploiting the strengths of different sensors in different situations and intelligently combining them.

An OG-map is a popular method of representing the environment for automotive and industrial applications [1-4]. In an OG map, the world surrounding the ego-vehicle is represented as a collection of equally sized cells contained within a rectangular grid. Each cell is assigned one or more numbers based on measurements made in the past and present, and each number represents the evidence supporting the state of a cell.

2-state OG maps are a widely used approach, in which each cell has one value, the probability of occupancy [1-4]. In these maps the probability of a cell being free is [1-probability of occupancy]. These probabilities are computed by accumulating instantaneous occupancy probabilities in to a map built over time. Instantaneous occupancy probabilities are computed from the raw sensor outputs and an inverse sensor model. The accumulation over time in these maps is typically based on an alpha filter. One of the shortcomings of these maps is that they don't quantify ambiguity, because the lack of evidence in occupancy is considered as evidence of empty space. Furthermore, these OG maps tend to suffer in the presence of moving objects [5].

A popular alternative to 2-state OG mapping is evidential OG mapping [5-7]. These maps typically are based on Dempster-Shafer theory [8]. With this approach, we can allow for more than 2 states, and we can also allow for ambiguous states, which are combinations of the defined states. For example, assume we define 3 states as: occupied with a dynamic object (D), occupied with a stationary object (S), and free (F). Then, the state space will include all the combinations of these states. This allows for us to define states such as SD, which means, we know there is evidence of an object, but we do not know if it is an object in motion.

In this paper, we describe an algorithm that we developed using inspiration from [5-7] to process inputs maps from multiple disparate sensors as they become available, to create a fused occupancy grid map that can handle dynamic objects. We use the Dempster-Shafer (DS) theory to construct this framework. By basing the algorithm on the DS theory we also allow for ambiguous states e.g. measurements made by a LIDAR sensor cannot be classified as stationary or dynamic, they can be either. Furthermore, instead of just one map, with this approach, we create multiple maps over time for the different states we are interested in.

We also detail an advanced inverse sensor model we developed for radar, specifically the TI mmWave sensor family, based on the gain profiles of the sensor according to angle and range. This model allows us to extract evidence for a cell being free and it being occupied by a dynamic or static object, whereas the previous model only provided evidence of a cell being occupied. It is important to note that a similar approach has been detailed in [3].

The structure of the paper is as follows: we will first describe conventional 2-state occupancy grid mapping, then evidential grid mapping as it relates to the problem of mapping, then inverse sensor models used for radar, LIDAR and camera, and finally we will show results for sensor fusion.

Conventional 2-State Occupancy Grid Mapping

In this section, we first describe sensor specific conventional 2-state OG mapping and then describe methods for fusing such maps to form a fused OG map.

A 2-state OG map is composed of a finite number of 2D-grid cells covering the area that needs to be mapped. At a given time k, a grid cell (i, j) is assigned a probability of occupancy $P_{i,j;0:k}^{occ}$. The probability of occupancy is typically computed using the instantaneous occupancy probability, $P_{i,j;k}^{occ}$, computed using sensor measurements at time k, and the occupancy probability accumulated from time 0 to $k-1$, $P_{i,j;0:k-1}^{occ}$. It is important to note that accumulation is not typically simple addition. Most commonly it is in the form of an alpha filter, where the past is weighted by α, and the present is weighted by $1-\alpha$, where $\alpha \in [0,1]$. Figure 1 illustrates this process. It is important to note that here "combine" refers to cell by cell accumulation. With this

model the probability of the cell being free is defined to be $\left(1 - P_{i,j;0:k}^{occ}\right)$.

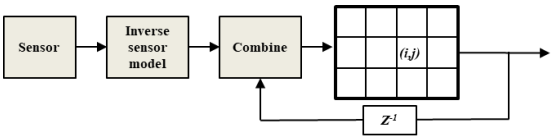

FIGURE 1: CONSTRUCTING A SENSOR SPECIFIC OG MAP.

Sensor specific OG maps can be fused in a variety of methods. One approach is to use sensor measurements to directly update a fused OG map, similar to the approach for sensor specific OG maps. Another, is to merge different sensor specific OG maps when they all become available, using a weighting scheme. In another, each cell is classified in sensor specific maps in to occupied, free or unknown. These maps are then combined using a fusion rule to form a fused map.

However, these OG maps do not perform well in the presence of moving objects, because they are not designed for such situations. Hence, in our work we utilize the evidential grid mapping approach instead because we can explicitly account for moving objects and also because it is conducive to sensor fusion.

Evidential Grid Mapping

In this section, we detail the multi-state evidential OG mapping approach we use for sensor fusion. We use DS theory to build the fundamentals of this approach and therefore we first explain the DS theory as it relates to the problem of mapping.

For this purpose, we first define the **frame of discernment,** Θ, as the set that contains all the states that we are interested in forming a belief about. For example, in the case of environment mapping we may have, $\Theta = \{O, F\}$, where, O stands for occupied and F stands for free. However, since we are interested in dynamic scenes as well, we define Θ as,

$$\Theta = \{S, D, F\} \tag{1}$$

where, S stands for static occupied, D stands for dynamic occupied and F stands for free. An element in the set Θ is known as a **focal element**.

Next we define the power set that corresponds to the frame of discernment as,

$$2^{\Theta} = \{\emptyset, S, D, F, SD, SF, DF, SDF\}. \tag{2}$$

Here, we notice that there are combinations of two states such as SD. Such states can model situations where we know the state if one of the two, but cannot distinguish exactly which. Hence, the state SD corresponds to the case when we know the state is either D or S but do not know exactly which. The ability to define such states is important for mapping because we have cases where we do not have sufficient evidence to distinguish between dynamic and stationary (e.g. radar measurement with zero Doppler, LIDAR measurements etc.).

The evidence for each of these states is given by the mass $m(\cdot) \in [0,1]$. According to DS theory, the masses for a given power set follow the law that: $\sum_{A \in 2^{\Theta}} m(A) = 1$. These masses may or may not be equal to the probability of the state.

In the case of grid mapping, our goal is to compute masses of these states for a given cell (i,j) for time k, $m_{i,j;0:k}(\cdot)$, using evidence from the sources available to us. In our problem, we have two sources of information – the previous masses of the cell, $m_{i,j;0:k-1}(\cdot)$, and the observation from the sensor at the current time, which gives us the mass $m_{i,j;k}^{m}(\cdot)$, which we will in future refer to as the measurement mass.

We can combine masses from these 2 sources using different methods available in the literature. One very popular method used in mapping is the **Dempster's method of combination** [6, 7, 9].

$$m_{i,j;0:k}(C) = \frac{\sum_{A \cap B = C \neq \emptyset;\, A \cap B \in 2^{\theta};\, A,B \neq \Theta} m_{i,j;0:k-1}(A) m_{i,j;k}^{m}(B)}{1 - K}, \tag{3}$$

Where,

$$K = \sum_{A \cap B \neq \emptyset} m_{i,j;0:k-1}(A) m_{i,j;k}^{m}(B). \tag{4}$$

However, we have concluded the through experimentation that this method of combination does not perform well in dynamic environments, and therefore we use the following method of combination [9]:

$$m_{i,j;0:k}(C) = \sum_{A \cap B = C \neq \emptyset;\, A \cap B \in 2^{\theta};\, A,B \neq \Theta} m_{i,j;0:k-1}(A) m_{i,j;k}^{m}(B) \tag{5}$$

It is important to note that there are other rules for combination that we have not implemented or described in this document that warrant further investigation [10-12]. Then, once the masses of the states are found, one can compute a resulting **Belief** about the state, which is defined as,

$$Bel(C) = \sum_{A | A \subseteq C \neq \emptyset;\, A \in 2^{\theta}} m_{i,j;0:k}(A) \tag{6}$$

In Figure 1 we show the DS-OG mapping algorithm for sensor fusion.

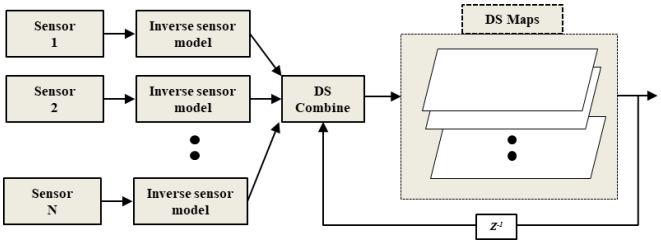

FIGURE 1: DS MAPPING FOR SENSOR FUSION

Here, the measurement masses come from N independent sensors, and are combined to the accumulated mass as they arrive. Next, we will describe how we compute the measurement mass from the measurements from each sensor.

Measurement Masses from Radar, LIDAR and Camera Sensor Measurements

In the next subsection, we describe how we obtain the instantaneous measurement masses for radar, LIDAR and camera. For this purpose, we will also explain the inverse sensor models we used for each modality. In this explanation, we will focus mostly

on our contributions to the inverse sensor models. It is also important to note that with these sensors, we are only able to compute evidence for states D, F and SD.

Radar Measurement Mass:

We start this section by explaining how we obtain the occupancy probability for a cell (i,j). Next, we explain how to compute the D, SD, and F measurement masses using the computed occupancy probability, the position of the cell with respect to measurements, the position of the cell with respect to the sensor (the gain profile of the TI mmWave sensor changes with angle and range), and the measured radial velocity.

Occupancy Probability of a Cell

In this section, we describe how we compute the occupancy probability from object level radar sensor data. We will not explain the procedure for obtaining object level data from raw radar sensor measurements because it is beyond the scope of this work.

When we refer to the object level data, we refer to the point-cloud that is generated from the raw radar sensor data. This point-cloud is a collection of points, where each point is described by its position, radial velocity and their ambiguities in the form of variance, in position and velocity. In particular, the point cloud at time k is the set, $R_k = \{l_1, \dots l_{N_k}\}$, where, l_m is one point, and N_k is the number of total points. A point l_m is described by c_{l_m}, v_{l_m} and Σ_{l_m}, where c_{l_m} are the polar coordinates of the point l_m with respect to the sensor, v_{l_m} is the radial velocity of the point w.r.t. the sensor and $\Sigma_{l_m} = \begin{bmatrix} \sigma^2_{r,l_m} & 0 \\ 0 & \sigma^2_{\theta,l_m} \end{bmatrix}$ where, σ^2_{r,l_m}, σ^2_{θ,l_m} are the variances of the measurement l_m in r and θ.

Using the object level data we define the occupancy probability for a cell $(i.j)$ as,

$$P^{occ,rad}_{i,j;k} = min\left\{ \sum_{l_m \in \partial R_{(i,j;k)}} \frac{a_{(i,j)}}{2\pi\sqrt{|\Sigma_{l_m}|}} exp\left\{ -\frac{1}{2}\left(c_{l_m} - c_{i,j}\right)^t \Sigma^{-1}_{l_m}\left(c_{l_m} - c_{i,j}\right)\right\}, 1\right\}. \quad (7)$$

Here, $\partial R_{(i,j;k)}$ is the set of points in the "neighborhood" of coordinates (i,j) and $a_{(i,j)}$ is the area of the cell. We define a neighborhood because the contributions from measurements that are considerable far away are negligible and only add to the computational cost. In practice, we do not iterate over the cells, rather, we iterate through the measurements, and update a block of predefined size using each measurement, to reduce computations. This team did not develop this portion of the algorithm; we describe it because it is necessary to explain how we compute the measurement masses per cell.

Measurement Mass from Occupancy Probability

Now we describe how we compute the measurement masses for $D, F, SD \in 2^\theta$. It is important to note that we can only derive evidence for SD and not for S, even though we know the radial velocity of a point. This is because the radial velocity is a projection of the actual velocity vector of a given point, in the radial direction. Furthermore, since we cannot compute measurement masses for S, SF and DF we set each to zero.

We iterate through the cells (i,j) at time k that are in the field of view (FOV) of the sensor and compute the measurement masses for said cells. A cell is considered to be in the FOV of the sensor if it satisfies the following two conditions:

1. the angle the cell makes with the normal to the sensor location is between $\pm\theta_{FOV}$
2. the cell is less than R_{FOV} away from the sensor.

Then, in the FOV we define 4 distinct regions and assign masses as described below:

- **If $P^{occ,rad}_{i,j;k}$ is greater than a threshold ϵ_{occ}:** we assume the cell has evidence of an object, and either the mass of SD or D must be positive. If the velocity computed for the cell, $v_{i,j;k}$ is greater than a threshold ϵ_v, then, we attribute the evidence to D, and otherwise to SD. In this implementation, $v_{i,j;k}$ is computed as follows:

$$v_{i,j;k} = \max_{l_m \in \partial R_{(i,j;k)}} \{v_{l_m}\}. \quad (8)$$

- **If $P^{occ,rad}_{i,j;k}$ is smaller than a threshold ϵ_{occ}:** we assume there is no evidence of an object. In that case, we want to know if the cell is either:
  - **In between the sensor and an occupied cell:** The assigned mass is constant, since we are quite certain another object is not present here.
  - **Not in a straight line that connects an occupied cell and the sensor or behind an occupied cell:** In these cases we weight the free space mass based on the sensor gain profile.

Table 1 illustrates these scenarios further.

Table 1: *Measurement masses of cells based on position with respect to sensor and measurements. Note, the length of arrows corresponds to the length of the velocity vector. Here, $\rho \in [0,1]$ is a constant, $w^{f,\theta}(\theta_{i,j:k})$ and $w^{f,r}(r_{i,j;k})$ are weights that reflect the sensor characteristics with respect to the angle and radial distance.*

	Visualization	$m^m_{i,j;k}(D)$	$m^m_{i,j;k}(SD)$	$m^m_{i,j;k}(F)$
Case 1: $P^{occ,rad}_{i,j;k} > \epsilon_{occ}$, $v_{i,j;k} > \epsilon_v$	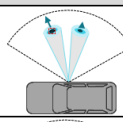	$P^{occ,rad}_{i,j;k}$	0	0
Case 2: $P^{occ,rad}_{i,j;k} > \epsilon_{occ}$, $v_{i,j;k} \leq \epsilon_v$	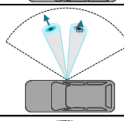	0	$P^{occ,rad}_{i,j;k}$	0
Case 3: $P^{occ,rad}_{i,j;k} \leq \epsilon_{occ}$, $v_{i,j;k} = 0$	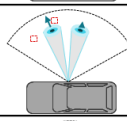	0	0	$\rho * w^{f,\theta}(\theta_{i,j;k}) * w^{f,r}(r_{i,j;k})$
Case 4: $P^{occ,rad}_{i,j;k} \leq \epsilon_{occ}$, $v_{i,j;k} = 0$	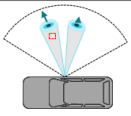	0	0	ρ

The weights $w^{f,\theta}(\theta_{i,j:k})$ and $w^{f,r}(r_{i,j;k})$ in the table are computed as shown below:

$$w^{f,\theta}(\alpha) = \begin{cases} cos\left(\frac{|\alpha| * 90}{\theta^f_{max}}\right) & if \alpha \leq \theta^f_{max} \\ 0 & o.w. \end{cases} \quad (9)$$

$$w^{f,r}(u) = \begin{cases} 1 & if\ u < r_1^f \\ e^{-b^f(u - r^f_{max})} & if\ r_1^f \leq u \leq r^f_{max} \\ 0 & o.w. \end{cases} \quad (10)$$

It is important to note that these profiles were chosen to correspond loosely to TI mmWave sensor characteristics. In the future we hope to replace these with a look up table based approach, in which the exact gain profiles will be used instead of the above approximations. It is important to note that a similar method is detailed in [2].

LIDAR Measurement Mass:

Once more, as in radar, we start explaining the procedure for computing the measurement mass starting from the point-cloud, since the processing prior to that is beyond the scope of this work. Here, a point is described by its position with respect to the sensor, and its class (obstacle/ground). In this implementation, we use the ratio between the number of points classified as ground points within a cell to the number of points classified as occupied within the same cell, to determine if a cell is occupied or free. Then, if it is deemed occupied we assign a constant measurement mass, $\rho^{occ,lid}$, to state SD, if it is deemed free we assign a constant measurement mass, $\rho^{free,lid}$, to the state F, and if not either, we set the measurement masses to 0.

Hence, we first compute:

$$\tilde{P}^{occ,lid}_{i,j;k} = \frac{N^{obj,lid}_{i,j;k}}{N^{grn,lid}_{i,j;k}} \quad (11)$$

where, $N^{grn,lid}_{i,j;k}$ is the number of points that are ground points and $N^{obj,lid}_{i,j;k}$ the number of points that are not ground points in cell (i,j). Then,

$$m^m_{i,j;k}(SD) = \mathbf{1}_{\left\{\tilde{P}^{occ,lid}_{i,j;k} > T_{occ,lid}\right\}} * \rho^{occ,lid} \quad (12)$$

where, $\rho^{occ,lid}$, $T_{occ,lid}$ are constants and $\mathbf{1}_{\{a>b\}}$ is an indicator function that is1 if $a > b$ and 0 otherwise. Then,

$$m^m_{i,j;k}(F) = \mathbf{1}_{\left\{\left(1/\tilde{P}^{occ,lid}_{i,j;k}\right) > T_{free,lid}\right\}} * \rho^{free,lid} \quad (13)$$

where, again $\rho^{free,lid}$ and $T_{free,lid}$ are constants. Finally, since we have no evidence of whether measurements are dynamic,

$$m^m_{i,j;k}(D) = 0 \quad (14)$$

Camera Measurement Mass:

Again, we start with the point-cloud generated by Structure From Motion (SFM) processing, and a point is described exactly as in LIDAR. In this implementation, we use the difference between the number of points classified as ground points within a cell to the number of points classified as occupied within the same cell, to determine if a cell is occupied or free. Then, if it is deemed occupied we assign a constant measurement mass, $\rho^{occ,cam}$, to state SD, if it is deemed free we assign a constant measurement mass, $\rho^{free,cam}$, to the state F, and if not either, we set the measurement masses to 0.

Hence, we first compute:

$$\tilde{P}^{occ,cam}_{i,j;k} = N^{grn,cam}_{i,j;k} - N^{obj,cam}_{i,j;k} \quad (15)$$

where, $N^{grn,cam}_{i,j;k}$ is the number of points that are ground points and $N^{obj,cam}_{i,j;k}$ the number of points that are not ground points in cell (i,j). Then,

$$m^m_{i,j;k}(SD) = \mathbf{1}_{\left\{-\tilde{P}^{occ,cam}_{i,j;k} > T_{occ,cam}\right\}} * \rho^{occ,cam} \quad (16)$$

where, $\rho^{occ,cam}$, $T_{occ,cam}$ are constants,

$$m^m_{i,j;k}(F) = \mathbf{1}_{\left\{\tilde{P}^{occ,cam}_{i,j;k} > T_{free,cam}\right\}} * \rho^{free,cam} \quad (17)$$

where, again $\rho^{free,cam}$ and $T_{free,cam}$ are constants. Finally, once again since we have no evidence of whether measurements are dynamic,

$$m^m_{i,j;k}(D) = 0 \quad (18)$$

Results

In this section, we first show results from fusing measurements from four radar sensors mounted on a vehicle using the approach described here (DS-OG mapping) and compare them to an accumulated two-state OG mapping approach we previously used. It is important to note that the 2-state OG mapping approach does not utilize the new Radar inverse sensor model, and as a result does not have a free space model, but, the DS-OG mapping approach utilizes the new Radar inverse sensor model. Then, we will show results from fusing 4 radars, a LIDAR and a camera sensor using the DS-OG mapping approach. It is important to note that in these results all three sensors use the inverse sensor models described in the previous sections.

Comparing 2-State OG Mapping and DS-OG Mapping for Surround Radar Fusion:

Here, we compare 2-state OG mapping with DS-OG mapping by comparing maps generated using measurements from four radar sensors. For the two experiments we describe below, we mount the sensors as shown in Figure 3, i.e. the first experiments uses configuration (A) and the second uses configuration (B).

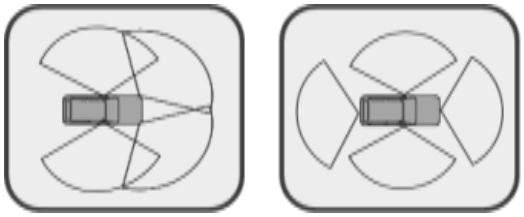

FIGURE 2: RADAR SENSOR CONFIGURATIONS. (A) ON LEFT: THE SENSORS ARE MOUNTED ON THE FRONT AND SIDES, (B) ON RIGHT: THE SENSORS ARE MOUNTED ON THE SIDES, BACK AND FRONT.

In the first experiment, the vehicle is moving through a parking lot with stationary vehicles. In the second experiment, in addition to the parked vehicles, we also have two moving objects:

a person moving across the road and a person moving a few meters to the East from the passenger side of the car. The results of the two experiments are shown in Figures 4 and 5 respectively. Since the first experiment has no moving objects we only show the SD map, $m_{i,j;0:k}(SD)$, for DS-OG mapping. Then, since there are moving object in the next experiment we show excerpts from the D map, $m_{i,j;0:k}(D)$, as well. In these figures, the color spectrum starts in blue for 0 and becomes more yellow as the values approach 1.

In Figure 4, we observe that with DS-OG mapping we get clearer and sharper boundaries of vehicles when compared to the traditional OG mapping. However, we do also see loss in detail with DS-OG mapping. In Figure 5, we observe that moving objects are not visible in the SD map and are only visible in the D map, whereas with 2-state OG mapping, streaks are left in the path of moving objects. These results clearly show the advantages of the DS-OG map when compared with the traditional OG map.

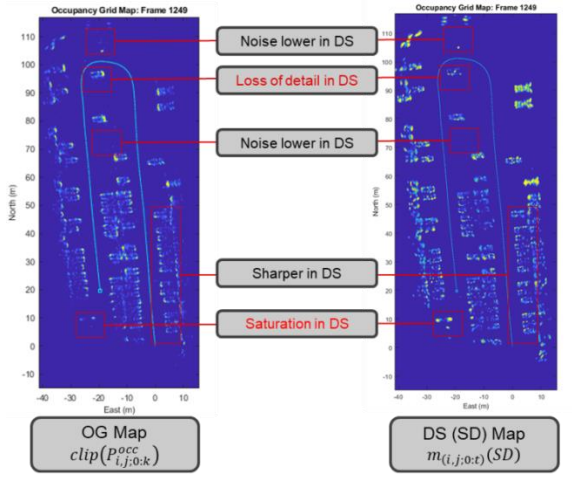

FIGURE 3: COMPARING CONVENTIONAL AND DS OG MAPS IN STATIC SCENE

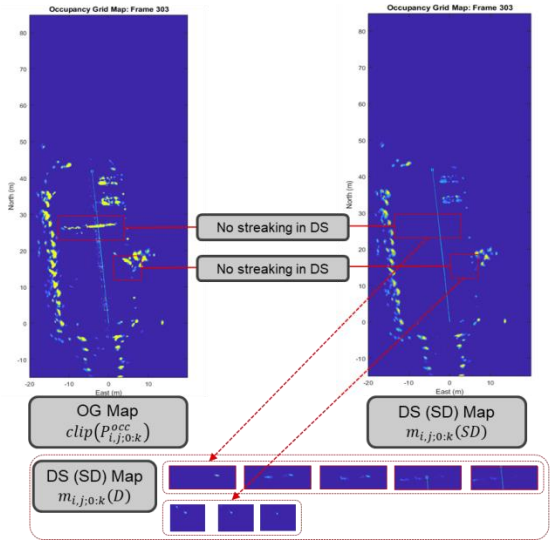

FIGURE 4: COMPARING CONVENTIONAL AND DS OG MAPS IN DYNAMIC SCENE

DS-OG Mapping for Disparate Sensor Fusion:

Here, we show results from DS-OG mapping applied to disparate sensor fusion. In particular, we fuse measurements from four radar sensors mounted according to Figure 3 (A), a LIDAR mounted on the roof of the vehicle and a Camera co-located with the passenger side Radar. Here, cyan is reserved for F, yellow for SD, and magenta for D. Again, as the mass increases the concentration of color increases. The sequence used here is the same as the one used to generate Figure 5.

The results of the experiment (4 frames from the sequence) are shown in Figure 5. It is evident from these figures that we can get a clear understanding of the surroundings with the DS based fusion approach. Furthermore, we also see that dynamic objects are visible and do not pollute the map. The reason we do not see concentrated magenta is because moving objects don't stay in a cell for long enough to get enough accumulation for concentrated magenta.

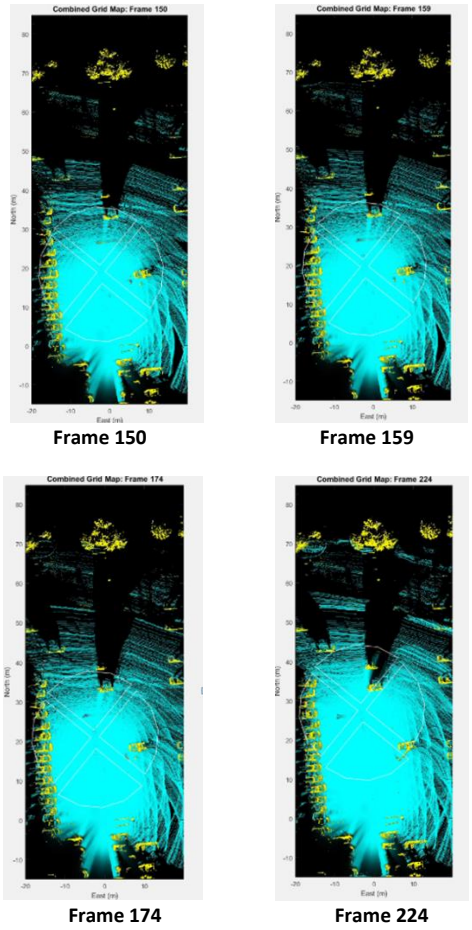

FIGURE 5: DS-OG MAPPING FOR SENSOR FUSION

Conclusion

In this paper, we have demonstrated that evidential grid mapping based on the Dempster-Shafter theory can be used for fusing measurements from multiple disparate sensors. We have also shown that our approach can handle moving objects in the scene better than 2-state OG maps, when used in tandem with the inverse radar sensor model described here. Furthermore, we have

shown that with an improved inverse sensor model, we can extract more information from radar measurements, and use this data for evidential grid mapping. We have implemented this code on the OpenVX framework and ported it on to an embedded platform. As future work, we plan to optimize the performance of the algorithm further.

References

[1] Thrun, Sebastian. "Robotic mapping: A survey." Exploring artificial intelligence in the new millennium 1, no. 1-35 (2002): 1.

[2] Dickmann, Juergen, et al. "Automotive radar the key technology for autonomous driving: From detection and ranging to environmental understanding." In 2016 IEEE Radar Conference (RadarConf), pp. 1-6. IEEE, 2016.

[3] Werber, Klaudius, et al. "Automotive radar gridmap representations." In 2015 IEEE MTT-S International Conference on Microwaves for Intelligent Mobility (ICMIM), pp. 1-4. IEEE, 2015.

[4] Godaliyadda, G. M, et al. "A Sense and Avoid Algorithm using Surround Stereo Vision for Drones." Electronic Imaging 2017, no. 19 (2017): 29-34.

[5] Pagac, Daniel et al. "An evidential approach to map-building for autonomous vehicles," IEEE Transactions on Robotics and Automation 14, no. 4 (1998): 623-629.

[6] Moras, Julien et al. "Moving objects detection by conflict analysis in evidential grids," Intelligent Vehicles Symposium (IV), 2011 IEEE, pp. 1122-1127. IEEE, 2011.

[7] Nguyen, Thien-Nghia et al. "Stereo-camera-based urban environment perception using occupancy grid and object tracking," IEEE Transactions on Intelligent Transportation Systems 13, no. 1 (2012): 154-165.

[8] Dempster, Arthur P. "Upper and lower probabilities induced by a multivalued mapping," The annals of mathematical statistics (1967): 325-339.

[9] Sentz, Kari et al.. “Combination of evidence in Dempster-Shafer theory,”.Vol. 4015. Albuquerque: Sandia National Laboratories, 2002.

[10] Yager, Ronald R. "On the Dempster-Shafer framework and new combination rules," Information sciences 41, no. 2 (1987): 93-137.

[11] Duan, Jianmin, et al. "Moving objects detection in evidential occupancy grids using laser radar," IHMSC, 2016 8th International Conference on. Vol. 2. IEEE, 2016.

[12] Jøsang, Audun. "The consensus operator for combining beliefs," Artificial Intelligence 141.1-2 (2002): 157-170.

Author Biographies

G. M. Dilshan Godaliyadda received his Ph.D. and Master’s degrees from Purdue University and his Bachelor’s degree from the University of Maryland. He joined Texas Instruments in 2018 and currently works as a Systems Engineer in the Systems R&D lab and is also as an Adjunct Professor at Southern Methodist University.

Vijay Pothukuchi received his Master’s degree in Computer Technology from Indian Institute of Technology, Delhi in 1997. He joined Texas Instrument in 2001 and currently works as Sr. Systems Architect in automotive and Radar systems & applications.

JuneChul Roh received his Ph.D. degree in Electrical and Computer Engineering from University of California, San Diego (UCSD) in 2005. Since then he joined Texas Instrument, and currently works as SMTS /Sr. Systems Architect in automotive and Radar systems & applications.

JOIN US AT THE NEXT EI!

IS&T International Symposium on

Electronic Imaging

SCIENCE AND TECHNOLOGY

Imaging across applications . . . Where industry and academia meet!

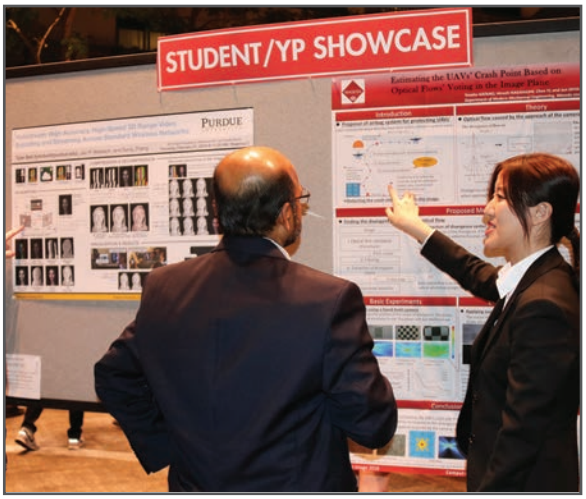

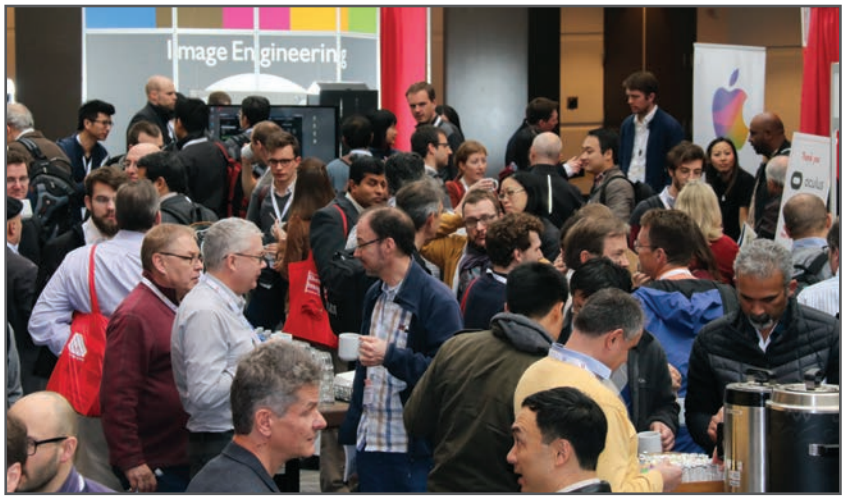

• SHORT COURSES • EXHIBITS • DEMONSTRATION SESSION • PLENARY TALKS •
• INTERACTIVE PAPER SESSION • SPECIAL EVENTS • TECHNICAL SESSIONS •

www.electronicimaging.org

IS&T
imaging.org